THE JOURNAL OF BIOLOGICAL CHEMISTRY Vol. 275, No. 16, Issue of April 21, pp. 11740–11749, 2000
Printed in U.S.A.

Magnesium-induced Linear Self-association of the FtsZ Bacterial Cell Division Protein Monomer

THE PRIMARY STEPS FOR FtsZ ASSEMBLY*

(Received for publication, October 20, 1999, and in revised form, January 11, 2000)

Germán Rivas‡§, Asunción López‡¶, Jesús Mingorance‖, María José Ferrándiz‖, Silvia Zorrilla‡, Allen P. Minton‡‡, Miguel Vicente‖, and José Manuel Andreu‡**

From the ‡Centro de Investigaciones Biológicas and ‖Centro Nacional de Biotecnología, Consejo Superior de Investigaciones Científicas, Madrid, Spain and ‡‡NIDDKD, National Institutes of Health, Bethesda, Maryland 20892

The bacterial cell division protein FtsZ from *Escherichia coli* has been purified with a new calcium precipitation method. The protein contains one GDP and one Mg^{2+} bound, it shows GTPase activity, and requires GTP and Mg^{2+} to polymerize into long thin filaments at pH 6.5. FtsZ, with moderate ionic strength and low Mg^{2+} concentrations, at pH 7.5, is a compact and globular monomer. Mg^{2+} induces FtsZ self-association into oligomers, which has been studied by sedimentation equilibrium over a wide range of Mg^{2+} and FtsZ concentrations. The oligomer formation mechanism is best described as an indefinite self-association, with binding of an additional Mg^{2+} for each FtsZ monomer added to the growing oligomer, and a slight gradual decrease of the affinity of addition of a protomer with increasing oligomer size. The sedimentation velocity of FtsZ oligomer populations is compatible with a linear single-stranded arrangement of FtsZ monomers and a spacing of 4 nm. It is proposed that these FtsZ oligomers and the polymers formed under assembly conditions share a similar axial interaction between monomers (like in the case of tubulin, the eukaryotic homolog of FtsZ). Similar mechanisms may apply to FtsZ assembly *in vivo*, but additional factors, such as macromolecular crowding, nucleoid occlusion, or specific interactions with other cellular components active in septation have to be invoked to explain FtsZ assembly into a division ring.

The FtsZ protein, which is found in all known eubacteria and archaea as well as in chloroplasts with the exception of the *Chlamydiae* (1, 2), plays a central role in bacterial cell division (3–5). During the life of a cell, FtsZ molecules remain in the cytoplasm until the time previous to division when they localize at the midcell point, forming a ring at the inner face of the cytoplasmic membrane where the septum will form (6, 7). The interactions of FtsZ with other septator proteins that are functionally relevant, such as PBP3 and FtsA, are being discovered (reviewed in Refs. 4, 5, 8, and 9). Several regulators of FtsZ ring formation have been found that either prevent/inhibit polymer formation (like the SOS response protein SulA (10), the MinCDE complex (11), and more recently, the ErzA protein from *Bacillus subtilis* (12)) or stabilize the FtsZ polymer (like the membrane protein ZipA (13, 14)). Despite this information, FtsZ ring structure and assembly are still poorly understood.

FtsZ binds guanine nucleotides and has GTPase activity (15–17), which is dependent on protein concentration and probably is linked to self-association equilibria (15, 16, 18). Multiple sequence alignment and secondary structure predictions indicate that bacterial FtsZ is a homolog of eukaryotic tubulins (19, 20). The x-ray crystal structure of the FtsZ from the archaeon *Methanococcus jannaschii* (21) and the electron crystallographic model structure of the $\alpha\beta$-tubulin dimer (22) have similar folds.

The nature of the polymers that FtsZ forms *in vivo* is unknown. FtsZ self-assembles *in vitro* to form filaments and rings (23–28). Electron microscopy studies of FtsZ filaments show that the longitudinal spacing in the polymers is close to the 4-nm spacing found in microtubules (23, 24). Similarly to microtubules (29) FtsZ assembly depends on divalent cations and guanine nucleotides and involves GTP hydrolysis (26). These physiological ligands have an important role in the control of the structure, associations, and assembly of tubulin. A high affinity Mg^{2+} bound to the non-hydrolyzable GTP of α-tubulin regulates the structural stability of the $\alpha\beta$ heterodimer (30). The hydrolyzable GTP bound to β-tubulin regulates tubulin assembly and microtubule dynamic instability, where several lower affinity Mg^{2+}-binding sites are also implicated (31–36). Tubulin exists into two conformational states as follows: the active (straight) conformation with GTP bound in the β-subunit (GTP-tubulin) which favors self-assembly into the physiological microtubule polymers (37–39), and the inactive (curved) GDP-bound state (36) which favors tubulin assembly into double rings over microtubule formation (33, 40–43).

The aim of the present work was to study FtsZ self-association in solution and the specific role of divalent cations. The processes of association and assembly seem to be relevant in the biological function of FtsZ. We have addressed the question whether the smallest association state of FtsZ in solution is a monomer or an oligomer. We have quantitatively characterized the effect of Mg^{2+} and Ca^{2+}, ionic strength, and guanine nucleotides on the self-association of *Escherichia coli* FtsZ by means of analytical centrifugation (sedimentation equilibrium and velocity), and we have investigated the nature of the oligomeric species.

EXPERIMENTAL PROCEDURES

Chemicals

$CaCl_2$, $MgCl_2$, EDTA, Tris, and glycerol, all of analytical grade, were from Merck. Guanine nucleotides, GDP and GTP, were from Sigma and Roche Molecular Biochemicals, respectively. *N*-Acetyltyrosinamide was from Serva; guanidine hydrochloride was from Calbiochem, and fluorescein 5′-isothiocyanate was from Molecular Probes Inc. Other analyt-

* This work was supported by Grants BIO99-0859-C03-02 (to J. M. A.), BIO99-0859-C03-03 (to G. R.), and BIO97-1246 (to M. V.) from Plan Nacional de I + D (Ministerio de Educación y Cultura, Spain) and EC DGXII Grant BIO-CT96-0122 (to M. V.). The costs of publication of this article were defrayed in part by the payment of page charges. This article must therefore be hereby marked "*advertisement*" in accordance with 18 U.S.C. Section 1734 solely to indicate this fact.

§ To whom correspondence should be addressed: Centro de Investigaciones Biológicas, CSIC, Velázquez 144, E-28006 Madrid, Spain. Fax: 34-91-562-7518; E-mail: grivas@cib.csic.es.

¶ CSIC predoctoral fellow.

** Postdoctoral fellow from the Comunidad Autónoma de Madrid.

ical grade chemicals were from Merck or Sigma, except as otherwise indicated.

FtsZ Purification

In order to optimize FtsZ purification, in terms of protein purity, yield, and nucleotide bound, two methods have been compared. The first of them (Method 1) is a modification of the standard FtsZ purification by precipitation of this protein with ammonium sulfate followed by ion exchange (17, 44). The second one (Method 2), developed in this work, takes into account the dependence of FtsZ solubility on divalent cations (28) and the methods of tubulin isolation by cycles of Mg^{2+}-induced association (45).

The steps of cell growth and lysis were essentially the same in both methods. Briefly, FtsZ was overproduced in *E. coli* BL21(DE3) transformed with the plasmid pMFV56, which contains the *E. coli ftsZ* gene cloned in a pET-28a vector (Novagen). Cells were grown at 37 °C in 1 liter of LB culture media (46) with kanamycin, to an A_{600} of 0.5–0.6. Expression was induced with 0.4 mM isopropyl-1-thio-β-D-galactopyranoside during 90 min (in Method 2, 180 min). Cells were harvested by centrifugation (10,000 × *g*, during 15 min at 4 °C), and pellets were resuspended either in 50 ml of Tris glycerol buffer (Tris glycerol buffer, 50 mM Tris-HCl, 50 mM KCl, 1 mM EDTA, 10% glycerol, pH 8.0) (Method 1) or in 20 ml of PEM buffer (PEM buffer, 50 mM PIPES,[1] 5 mM $MgCl_2$, 1 mM EDTA, pH 6.5) (Method 2), and then the cells were lysed on ice using an MSE sonicator. The soluble fraction, containing the FtsZ protein, was separated from the cell debris by centrifugation (100,000 × *g*, for 2 h at 4 °C).

In Method 1, the protein from the soluble fraction was precipitated with 30% ammonium sulfate. The sample was centrifuged (50,000 × *g*, for 35 min at 4 °C), and the pellet was resuspended in 5 ml of Tris glycerol buffer. In Method 2, the protein was extracted by two cycles of Ca^{2+}-induced precipitation. In the first cycle, 1 mM GTP and 20 mM $CaCl_2$ were added to the solution, and the sample was incubated during 15 min at 30 °C and then centrifuged (11,000 × *g*, for 15 min at 4 °C). The pellet, which contains FtsZ, was resuspended in 20 ml of PEM buffer and centrifuged as in the previous step to eliminate any insoluble material. The supernatant was subjected to an identical second cycle of Ca^{2+}-induced precipitation. The final FtsZ pellet was resuspended in 5 ml of PEM buffer.

The materials from the previous step, highly enriched in FtsZ protein but contaminated with nucleic acid, were further purified by anion exchange chromatography using a 5-ml Hi-Trap Q-Sepharose column (in an Amersham Pharmacia Biotech FPLC system, at a flow rate of 1 ml/min), equilibrated in Tris glycerol buffer either without adding $MgCl_2$ (Method 1) or with 5 mM $MgCl_2$ (Method 2). FtsZ, due to its negative charge, was retained in the column and was eluted with a 0–100% gradient of 1 M KCl in the same buffer. In both cases the protein eluted around 500–600 mM KCl. The purified FtsZ aliquots were dialyzed either in Tris-200KCl buffer with 1 mM EDTA and 10% glycerol (Method 1) or in Tris-250KCl buffer with 10% glycerol (Method 2) and stored at −80 °C. We have chosen Method 2 to isolate FtsZ because of the following: (i) the purity in SDS-PAGE was >98%, whereas was only >95% for Method 1; (ii) the stoichiometry of nucleotide binding was also higher for FtsZ purified using Method 2 (1.1 ± 0.1 mol of bound GDP/mol of FtsZ, whereas only 0.6 ± 0.1 for FtsZ Method 1); and (iii) the protein yield (~40 mg of protein/liter culture) was higher than that obtained with Method 1 (~20 mg/liter). The GTPase activity of FtsZ purified by both methods was ~120 nmol $P_i \cdot min^{-1} \cdot mg^{-1}$, which corresponds to 5 molecules of GTP hydrolyzed at 37 °C per min and molecule of FtsZ (at 5 μM protein).

Protein and Nucleotide Quantitation

The determination of FtsZ concentration is not straightforward because the *E. coli* protein has few aromatic residues (only three tyrosines and no tryptophans (47)), and the bound nucleotide dominates the UV absorption spectrum. The nucleotide content of the protein was determined, after extraction with perchloric acid, by HPLC with an internal standard of guanosine, using an extinction coefficient of guanine nucleotides at 254 nm of 12,400 M^{-1} cm^{-1} (31, 48). Two methods were employed to measure accurately the concentration of FtsZ at a given wavelength in the desired working buffer. This is important, for example, to measure the protein concentration gradients in analytical centrifugation experiments.

UV Spectroscopy—FtsZ concentration was first measured by taking its UV spectra in 6 M GdnHCl. From these spectra the concentration of the protein (which has three Tyr) was calculated after subtracting the GDP contribution at 280 nm, using the following molar extinction coefficients: 1280 M^{-1} cm^{-1} for Tyr (49, 50) and 8,100 M^{-1} cm^{-1} for GDP.[2] Comparison with the spectra in 50 mM Tris-HCl, 50 mM KCl, pH 7.5, buffer yielded practical molar extinction coefficients for the native protein-GDP complex at 280 (13,800 ± 900 M^{-1} cm^{-1}) and 254 nm (17,100 ± 1,100 M^{-1} cm^{-1}). Note that these coefficients are only valid for FtsZ which has 1.1 ± 0.1 molecules of bound GDP.

Fluorescence Spectroscopy—The intrinsic fluorescence signal of the Tyr residues of FtsZ was used to quantify FtsZ at low concentrations, since the emission spectra of the protein showed no fluorescent contaminants. The spectrofluorimetric measurements of FtsZ samples (diluted to <5 μM to avoid inner filter effects) in 6 M GdnHCl were performed at 20 °C in a Shimadzu RF-540 fluorimeter (λ_{ex} = 275 nm; λ_{em} = 305 nm), with 0.5 × 1 cm cells, using *N*-acetyltyrosinamide (1–40 μM) as standard. This simple procedure gave the same results as UV spectroscopy within experimental error.

Quantitative amino acid analysis (51) was used to confirm the FtsZ quantitation methods previously described. The amino acid content of the protein was measured after acid hydrolysis (6 N HCl with norleucine as internal standard, at 110 °C, during 20 h) in a Beckman 630 automatic amino acid analyzer. The amino acid composition, in particular the number of phenylalanine and tyrosine residues, was in agreement with that calculated from the *E. coli* FtsZ gene sequence (47). By taking into account the total amino acid residues of FtsZ from sequence (as well as using the content of several reference residues, like alanine, glutamine + glutamate, and asparagine + aspartate), the number of moles of FtsZ in the original sample was calculated. This method understimated the FtsZ concentration by around 10% with respect to the spectrophotometric method. Finally, a colorimetric protein assay, using the Coomassie Brilliant Blue G-25 reagent (Bio-Rad) had, in our hands, a poor reproducibility and overestimated the FtsZ content around 20%.

Determination of FtsZ-bound Mg^{2+} and Ca^{2+}

The divalent cation content of FtsZ was measured in aliquots of 2 ml (25–50 μM) either directly from the stock solution stored in Tris glycerol buffer or after equilibrium dialysis in Tris-50KCl buffer (Tris-50KCl buffer, 50 mM Tris-HCl, 50 mM KCl, pH 7.5) at 20 °C. Measurements were performed by atomic absorption spectroscopy (52) and by inductively coupled plasma optical emission spectroscopy (53). Standard solutions of Mg^{2+} were purchased from Sigma, and Ca^{2+} stock solutions were prepared from a known amount of $CaCO_3$. Only plasticware containers were employed, and all the solutions were prepared with fresh MilliQ grade water (Millipore Inc.).

Specific GTPase Activity

The GTPase activity of FtsZ (5 μM in Tris-100KCl buffer with 5 mM $MgCl_2$ and 0.5 mM GTP) was measured at 37 °C by quantitation of the inorganic phosphate with the malachite green-molybdate reagent (54, 55).

FtsZ Polymerization

The formation of large FtsZ polymers, after incubation of the protein (~12.5 μM, in MES buffer (MES buffer, 50 mM MES-KOH, 50 mM KCl, pH 6.5)) with 1 mM GTP and 10 mM $MgCl_2$ at 30 °C, was followed by 90° angle light scattering monitored with a High-Tech Scientific SS-51 stopped-flow device with a fluorescence detection system, employing 350 nm incident light and a filter with a cut-off below 330 nm for the scattered light. The dead time of the instrument was 2.5 ms, calibrated with the reaction of *N*-bromosuccinimide with *N*-acetyltryptophanamide (56). Light scattering at 90° was also monitored, using a Shimadzu RF-540 fluorimeter. FtsZ polymers were adsorbed to

[1] The abbreviations used are: PIPES, piperazine-*N*,*N*′-bis(2-ethanesulfonic acid); MES, 4-morpholineethanesulfonic acid; FITC, fluorescein 5′-isothiocyanate; HPLC, high performance liquid chromatography; GdnHCl, guanidine hydrochloride; $\overline{M}_w$, weight average molecular weight.

[2] J. M. Andreu and J. F. Díaz, unpublished data.

carbon-coated grids, negatively stained with 2% uranyl acetate, and inspected with a Jeol 1200 EX electron microscope.

Analytical Centrifugation

Sedimentation equilibrium experiments were performed at 20 °C in an Optima XL-A (Beckman-Coulter) analytical ultracentrifuge equipped with UV-visible optics, using An50Ti and An60Ti rotors, with either 12-mm double sector or six-channel centerpieces of Epon charcoal. FtsZ (loading concentration between 5 and 100 μM) was equilibrated in Tris-50KCl buffer, with 20 μM GDP and the desired concentration of divalent cations and KCl, except otherwise indicated (*i.e.* experiments at pH 6.5 in PIPES or MES buffers). Omission of GDP in the buffer resulted in the partial dissociation of the GDP bound to the protein within the experiment time interval. Short column (50–60 μl), low speed sedimentation equilibrium was performed at three successive speeds (5, 8, and 15,000 rpm), and the equilibrium scans were taken (typically after 10 h) at the most appropriate wavelength (240, 280, or 290 nm), depending upon the FtsZ concentration. Attention was given to the conservation of protein mass in soluble form during the experiment, and control sedimentation velocity experiments showed no aggregation within a 12-h time interval. In all cases, the base-line signals were measured after high speed centrifugation (40,000 rpm). Whole-cell apparent weight average molecular weights of FtsZ were obtained using the program EQASSOC (57). The partial specific volume of FtsZ was 0.738 ml/g, calculated from the amino acid composition with the program SEDNTERP (retrieved from the RASMB server (58)). In order to quantitatively characterize the effect of Mg^{2+} on FtsZ self-association, the dependence of the weight average molecular weight ($\overline{M}_w$) of FtsZ on protein concentration was calculated[3] from the local slopes of the transformed linearized data (ln *c versus* r^2) at defined radial intervals (57). Data from different loading protein concentrations and equilibrium speeds were superimposed and averaged over an interval of $\pm$0.1 log concentration units (59).

Sedimentation velocity experiments were performed at 20 °C on parallel samples at 30,000, 40,000, and 50,000 rpm. Sedimentation coefficients were calculated either from the rate of movement of the solute boundaries, using the program XLAVEL (supplied by Beckman), or by globally fitting of multiple sedimentation velocity profiles with the program SVEDBERG (retrieved from the RASMB server (60)). From both methods we obtained similar apparent sedimentation coefficient values, which correspond to the maxima of the distribution of the apparent sedimentation coefficients, $g(s^*)$, calculated with the program DCDT (61), also taken from the RASMB server. The average sedimentation coefficients were calculated by integration as shown in Equation 1.

$$s_w = \frac{\int_0^\infty s * g(s^*)ds^*}{\int_0^\infty g(s^*)ds^*} \qquad \text{(Eq. 1)}$$

(See for example Ref. 62.) These coefficients were corrected to standard conditions to get the corresponding $s_{20,w}$ values using the SEDNTERP program.

Nonlinear Least Squares Modeling of Data

Different self-association models containing adjustable parameters (see under "Theory") were fitted to the weight average molecular weight *versus* concentration data via Marquardt-Levenberg minimization of χ^2 (63). Goodness of fit was evaluated from the statistical distribution of χ^2 for an identical number of degrees of freedom (see Chapter 14 of Ref. 63).[3]

Circular Dichroism

The far-UV circular dichroism spectra of FtsZ (5–50 μM, equilibrated in Tris-50KCl buffer, with 20 μM GDP and a known concentration of $MgCl_2$) were acquired at 20 °C in a JASCO J720 dichrograph, using 0.1- and 0.01-cm cells. Changes in FtsZ secondary structure were estimated by deconvolution of the CD spectra using Yang (64) and LIMCOMB (65) methods, as described (19).

[3] The Turbo Pascal source code for this calculation and the MS-DOS executable program and the MATLAB scripts are available from one of the authors (A. Minton) upon request.

Nucleotide Exchange

The nucleotide bound to FtsZ was exchanged by incubating GDP-FtsZ with a large molar excess of GTP and further removal of the unbound nucleotides by gel filtration, as described for tubulin (48). In the case of FtsZ, the gel filtration step was performed in Tris-50KCl buffer, with only 50 μM GTP, which permits us to follow the protein with the absorption optics in an analytical centrifuge.

Fluorescent Labeling of FtsZ

FITC labeling of FtsZ was performed essentially as described (66). Briefly, FtsZ (~30 μM) equilibrated in 20 mM phosphate, 10 mM $MgCl_2$, pH 8.0, was incubated with the fluorophore (~20 mol FITC/mol FtsZ) during 20–30 min at 20 °C. The unincorporated dye was separated from the labeled protein by gel filtration using a HiTrap desalting column (Amersham Pharmacia Biotech) equilibrated in Tris-50KCl buffer. The degree of labeling (~1–2 fluorescein/FtsZ) was determined spectrophotometrically.

Other Methods

The purity of FtsZ was checked by SDS-polyacrylamide gel electrophoresis performed essentially as described (19). Molecular weight markers from Amersham Pharmacia Biotech were employed. Gels containing 10% polyacrylamide were stained with Coomassie Blue. Microdensitometric scans of the gels were obtained with an Scanjet 6100c/T scanner (Hewlett-Packard) and analyzed with the program Scion Image (National Institutes of Health, Bethesda).

THEORY

Magnesium-dependent Indefinite Protein Self-association—Consider a protein molecule (A) with molar mass M_1, that self-associates according to the following series of stepwise indefinite self-association equilibria shown in Equation 2.

$$A_{i-1} + A = A_i \qquad \text{(Eq. 2)}$$

We may define the apparent stepwise association constant K_i as shown in Equation 3,

$$K_i = c_i/(c_1 \cdot c_{i-1}) \qquad \text{(Eq. 3)}$$

where $i = 2, 3, 4, \ldots$, and c_i is the molar concentration of i-mer. According to linkage theory (67–69), the effect of Mg^{2+} on the equilibrium constant is shown in Equation 4.

$$\ln K_i(c_{Mg}) = \ln K_i^* + n_i \ln(c_{Mg}/c_{Mg}^*) \qquad \text{(Eq. 4)}$$

where K_i^* is the value of K_i at a reference Mg^{2+} concentration c_{Mg}^* (1 mM in the present treatment), and n_i is the net uptake of Mg^{2+} upon the addition of 1 mol of FtsZ to a mole of $(i - 1)$-mer, which remains constant within the Mg^{2+} concentration range employed. It will be assumed in the present treatment that $n_i = n$ for all i and subsequently shown (see "Results") that this assumption satisfactorily accommodates the data.

It follows from Equation 3 that the concentration of each species is related to the monomer concentration by Equation 5,

$$c_i = Z_i c_1^i \qquad \text{(Eq. 5)}$$

where Z_i is a cumulative association constant shown in Equation 6.

$$Z_i \equiv \prod_{j=2}^{i} K_j \qquad \text{(Eq. 6)}$$

The standard state free energy change associated with the assembly of one i-mer from i protomers is given by Equation 7.

$$\Delta G_{1i} = \sum_{j=2}^{i} \Delta G_j = -RT \ln Z_i \qquad \text{(Eq. 7)}$$

The total concentration of protein expressed in moles of protomer per liter is then given by Equation 8.

$$c_{tot} = \sum_{i=1}^{\infty} ic_i = \sum_{i=1}^{\infty} (iZ_i c_1^i) \quad \text{(Eq. 8)}$$

Theoretical consideration of the energetics of indefinite linear self-association (70) suggests that the value of K_i should tend toward an asymptotic limit K_{inf} at sufficiently large oligomer size. For convenience, we denote by F_i the dimensionless ratio K_i/K_{inf}. Upon substitution of variables, Equation 8 may then be rewritten as Equation 9.

$$K_{inf}c_{tot} = \sum_{i=1}^{\infty} (i(K_{inf}c_1)^i \prod_{j=2}^{i} F_j) \quad \text{(Eq. 9)}$$

Given the values of c_{tot}, K_{inf}, and the F_j, Equation 9 may be solved (either analytically or numerically) for c_1 and subsequently for all c_i. The weight average molecular weight may then be obtained from Equation 10.

$$\bar{M}_w/M_1 = \sum_{i=1}^{\infty} i^2 c_i / c_{tot} \quad \text{(Eq. 10)}$$

Empirical Models for the Dependence of F_i (or K_i) on i—The following two functions provide a gradual variation of K_i from K_2 toward an asymptotic limit of K_{inf} in the limit of large i.

For an inverse decay model we get Equation 11.

$$F_i = 1 + \left[\frac{(J-1)}{(i-1)^{\alpha}}\right] \quad \text{(Eq. 11)}$$

For an exponential decay model we get Equation 12.

$$F_i = 1 + (J-1)\exp\left[\frac{-(i-2)}{\beta}\right] \quad \text{(Eq. 12)}$$

where $J = K_2/K_{inf}$, and α and β are empirical parameters characterizing the decay in their respective models. It will be shown subsequently that the dependence of association constants on the size of the aggregate derived from analysis of the experimental data is insensitive to the particular empirical model employed, so long as that model accurately describes the observed dependence of $\bar{M}_w/M_1$ on total protein concentration.

Simulation of the Dependence of s_w/s_1 on the Concentration of Protein—The weight average sedimentation coefficient is related to the sedimentation coefficients of individual sedimenting species, s_i, by Equation 13.

$$s_w = \frac{\sum_{i=1}^{\infty} ic_i s_i}{\sum_{i=1}^{\infty} ic_i} \quad \text{(Eq. 13)}$$

Estimates of c_i are obtained from the best fit of equilibrium self-association models to the dependence of $\bar{M}_w/M_1$ on protein and Mg^{2+} concentration, as described above, on the assumption that chemical equilibrium is achieved rapidly with respect to net transport in the sedimenting system. Estimates of s_i are obtained from structural models of oligomers together with simple calculations using Kirkwood's frictional theory (71, 72). The relationship between the sedimentation coefficient and oligomer size for different aggregate geometries (single and double-stranded linear oligomers) for identical spherical subunits is given by Equation 14 (71, 72).

$$s_i/s_1 = 1 + [(R_S/i)\Sigma\Sigma(1/R_{jk})] \quad \text{(Eq. 14)}$$

where s_i is the sedimentation coefficient for i associated subunits in the oligomer, s_1 is the sedimentation coefficient of the monomer, R_S is the Stokes' radius of FtsZ monomer (2.3 nm) and R_{jk} is the distance between subunits j and k, for all subunits in the oligomer. The known spacings between FtsZ subunits for Ca^{2+}-induced FtsZ polymers are an axial spacing of 4.3 nm and a lateral spacing of 3.5 nm (24). The dimensions reported for FtsZ polymers induced in the presence of DEAE-dextran and cationic lipids (23) are an axial spacing of 4.1–4.3 nm and an inter-protofilament spacing of ~5.3 nm (DEAE-dextran) and ~3.7 nm (cationic lipids). In the present simulations the spacings used were 4.3 and 6 nm. The values of s_i calculated from Equation 14 were compared with those based upon the simple approximation that all oligomers are spherical (72).

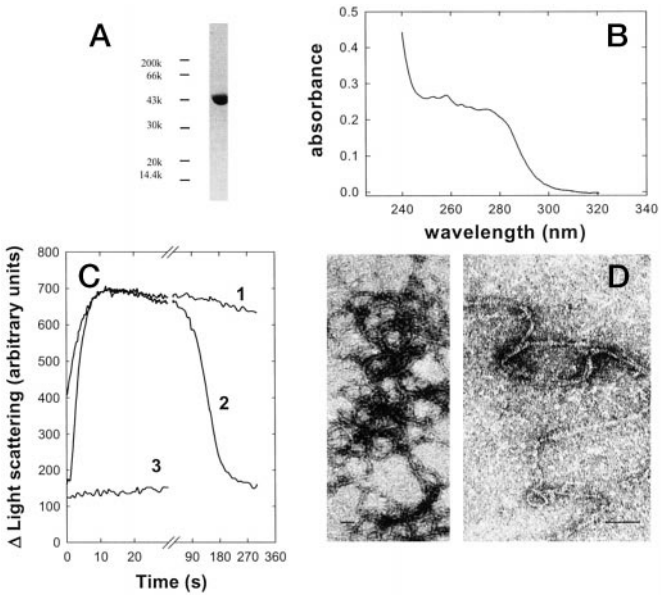

FIG. 1. **Biochemical characterization of *E. coli* GDP-FtsZ.** *Panel A,* SDS-PAGE of FtsZ. *Panel B,* UV spectra of FtsZ in Tris-KCl buffer. *Panel C,* assembly of FtsZ monitored with stopped-flow light scattering at 30 °C. The FtsZ solution (final concentration 12.5 μM in MES buffer) was made 10 mM $MgCl_2$ and either 1 mM GTP (*trace 1*), 0.1 mM GTP (*trace 2*), or 0 mM GTP (*trace 3*). *Panel D,* electron micrographs of negatively stained FtsZ polymers. The *bars* indicate 50 nm.

RESULTS

Functional Properties of Purified FtsZ—Overproduced *E. coli* FtsZ was purified with a new method employing cycles of Ca^{2+}-induced protein precipitation that was based on tubulin purification procedures. This method compares with advantage to conventional FtsZ purification protocols (see "Experimental Procedures"). Purified FtsZ (Fig. 1, *panel A*) has 1 mol of bound GDP (but no GTP or GMP) and 1 mol of bound Mg^{2+} per mol of protein, negligible Ca^{2+} bound,[4] and it has functionally normal GTPase activity. The unusual UV absorption spectrum of purified FtsZ (Fig. 1, *panel B*), corresponding to its chemical composition, is dominated by the contribution of bound GDP. The vibrational absorption bands of phenylalanine (251, 257, 263, and 267 nm (49)), the absorption maximum of tyrosine (275 nm), and the lack of Trp residues can be appreciated.

FtsZ assembly was induced by GTP and Mg^{2+} in MES buffer at 30 °C and was monitored by stopped-flow light scattering. The polymers formed in a few seconds, disassembled upon GTP consumption (Fig. 1, *panel C*), and did not form with 1 mM GDP to 10 mM $MgCl_2$ (not shown). The polymers observed with negative stain electron microscopy consisted of thin filaments of variable length and curvature. They were apparently single-

[4] Our divalent cation-free buffers typically contain 0.9 ± 0.2 and <10 ± 2 μM residual Mg^{2+} and Ca^{2+} concentrations, respectively.

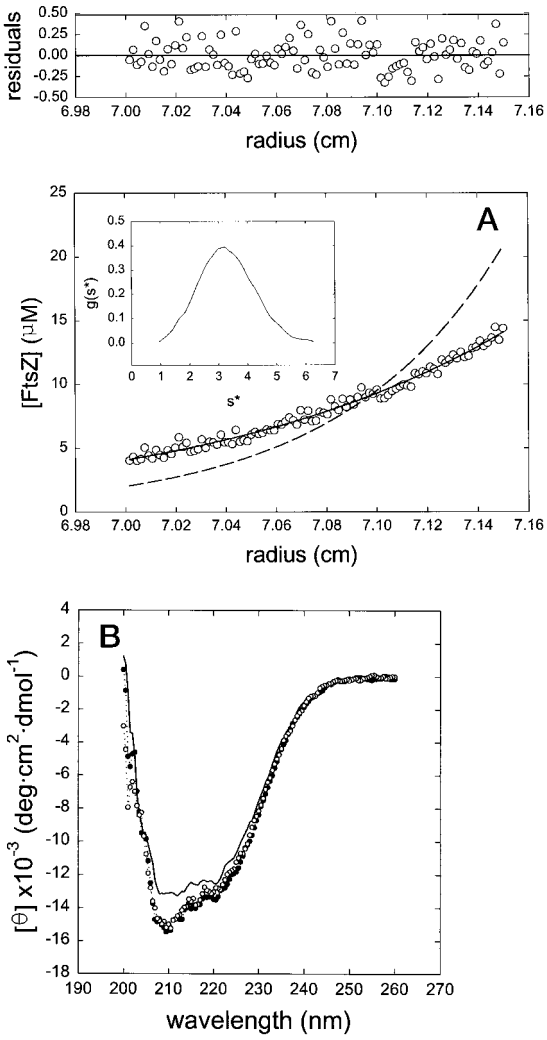

FIG. 2. **The FtsZ monomer.** *Panel A,* sedimentation equilibrium gradient of FtsZ monomer (8 μM in Tris-50KCl buffer with 20 μM GDP) at 8,000 rpm and 20 °C. *Open circles* represent the experimental data; the *solid line* is the best fit $\bar{M}_w$ (41,000 ± 3,000); the *dashed line* is the theoretical gradient of an FtsZ dimer (80,600). *Inset,* sedimentation velocity (50,000 rpm, 20 °C) distributions of the same FtsZ showed in the main figure. *Panel B,* effect of Mg^{2+} on the far-UV CD spectrum of FtsZ (5 μM). Mg^{2+} concentrations are ~1 μM (*solid line*), 1 mM (*open circles*), and 10 mM (*closed circles*). Each spectrum represents an average of five scans.

and double-stranded, ~5 and ~10 nm wide, respectively (Fig. 1, *panel D*). FtsZ polymer solutions had a very small turbidity (typically $\Delta A_{350\ nm,1\ cm} \leq 0.05$), like in the case of 6-nm actin filaments (73, 74). These observations are qualitatively compatible with a recent report on the assembly of ~7-nm wide FtsZ polymers (27) and thin filaments previously observed (75). However, significantly thicker FtsZ polymers, such as ~20 nm wide polymers (27), filaments induced by DEAE-dextran (23), or >50 nm wide Ca^{2+}-induced protofilament bundles (28), if they had been abundant in our solution, would have given a larger turbidity signal, similarly to microtubules (76).

The FtsZ Monomer—The nature of the smallest association state of FtsZ was studied under different solution conditions. In Fig. 2, *panel A*, the sedimentation equilibrium gradient of 8 μM FtsZ equilibrated in Tris-50KCl buffer (~1 μM residual free Mg^{2+}) is shown. The experimental data are best fit by a single exponential gradient with an apparent weight average molecular weight of 40,800 ± 2,400, which corresponds to the sequence molecular weight of FtsZ monomer (40,300). In sedimentation velocity experiments the same FtsZ sample sediments as a single homogeneous species of 3.4 ± 0.1 S (*inset* in Fig. 2**,** *panel A*), which is compatible with a globular FtsZ monomer of relative frictional ratio of 1.1 ± 0.1. At 25 μM FtsZ, the $\bar{M}_w$ was slighty higher (51,000), and the residuals distribution of the best fit was typical of an associating system (not shown). This behavior was confirmed with experiments at higher protein concentration (see Fig. 3, *panel A*), and it is in agreement with the increase of FtsZ sedimentation coefficient with protein concentration (see below, Fig. 6, *panel B*). From these experiments we concluded that FtsZ in solution is a globular monomer with a tendency to self-associate.

The secondary structure of FtsZ was checked by circular dichroism (CD) spectroscopy (Fig. 2, *panel B*). The spectra, characteristic of an α/β protein, showed an small increase (~10%) in the 210–220 nm CD signal with 1–10 mM $MgCl_2$ with respect to ~1 μM cation, which is compatible with an ~5–10% increase in the α-helical content induced by mM $MgCl_2$. This CD change was independent on FtsZ concentration (5–50 μM range, not shown), which suggests that it is linked to cation binding more than to protein association.

Mg^{2+}-induced FtsZ Self-association—The effect of Mg^{2+} on the self-association of FtsZ was studied by means of low speed sedimentation equilibrium over a broad range of protein (5–100 μM) and Mg^{2+} (~1 μM-10 mM) concentrations, in Tris-50KCl buffer at 20 °C. Sedimentation equilibrium gradients of FtsZ at a single protein concentration (75 μM) and multiple Mg^{2+} concentrations are shown in Fig. 3. In order to show the trend of the data, the corresponding best fit gradients for a single sedimenting species are also plotted. It is apparent upon inspection of the graphs that the molecular weight of FtsZ is increasing with increasing Mg^{2+} concentration. The protein gradient at 1 μM Mg^{2+} is very shallow, and the single species best fit $\bar{M}_w$ is ~69,000, a value 1.7 times larger than the corresponding to the sequence monomer molecular weight. At the highest Mg^{2+} concentration (10 mM) the gradient is steep, corresponding to a best fit $\bar{M}_w$ of ~390,000, but with a poor fit that indicates that the sample is heterogeneous in size. The dependence of $\bar{M}_w$ upon protein and Mg^{2+} concentrations, calculated as described under "Experimental Procedures," from these and many other data sets (not shown), is plotted in Fig. 4 (*panel A*). At high protein and Mg^{2+} concentrations, $\bar{M}_w$ approaches ~10 times that of the FtsZ monomer, and there is no hint of any asymptotic upper limit to $\bar{M}_w$. Such behavior is characteristic of an indefinite self-association.

Model Analysis of FtsZ Association—The empirical models for indefinite self-association described above under "Theory" (Equations 4 and 9–12) provide a satisfactory description, to within experimental precision, of the *combined* experimental data ($\bar{M}_w/M_1$ *versus* [FtsZ] at four Mg^{2+} concentrations: 1, 2, 5, and 10 mM) with four adjustable parameters. Two of the parameters, the dimensionless ratio J ($\equiv K_2/K_{inf}$) and the decay parameter (either α or β), describe a gradual reduction of the stepwise association constant K_i toward an asymptotic value K_{inf} in the limit of sufficiently large oligomer size. The parameter K^*_{inf} is an offset whose value depends upon the definition of the standard reference state, and the parameter n describes the linkage between protein association and Mg^{2+} uptake (Equation 4). The dependences of $\bar{M}_w/M_1$ on protein and Mg^{2+} concentrations, calculated from the best least square fits of both indefinite self-association models to the combined data (which are visually indistinguishable) is plotted together with the data in Fig. 4 (*panel A*), and the best fit parameter values are given in the figure legend. Four salient points emerge from our results.

1. The parameter n is constrained to a narrow set of values around 1 (n = 0.93 ± 0.2, 95% confidence limits), indicating

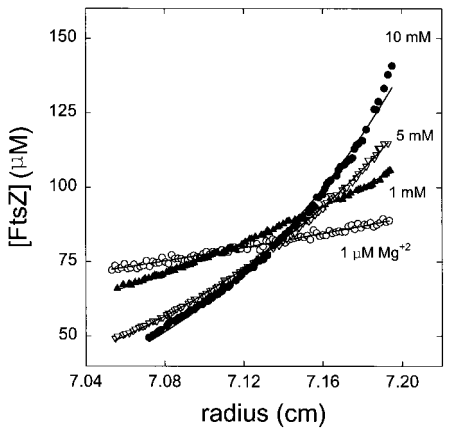

FIG. 3. **Mg^{2+}-induced FtsZ association.** Sedimentation equilibrium gradients of FtsZ (loading concentration 75 μM in Tris-50KCl buffer with 20 μM GDP; 5,000 rpm, 20 °C) at different Mg^{2+} concentrations: ~1 μM (*open circles*), 1 mM (*closed triangles*), 5 mM (*open inverted triangles*), and 10 mM (*closed circles*) Mg^{2+}. To show the trend of the data the best fit $\bar{M}_w$ for a single sedimenting species at the four Mg^{2+} concentrations represented in the figure are plotted as *solid lines*; the corresponding $\bar{M}_w$ values are as follows: 69,000 ± 4,500 (~1 μM Mg^{2+}), 163,000 ± 16,000 (1 mM Mg^{2+}), 298,000 ± 27,000 (5 mM Mg^{2+}), and 387,000 ± 31,000 (10 mM Mg^{2+}).

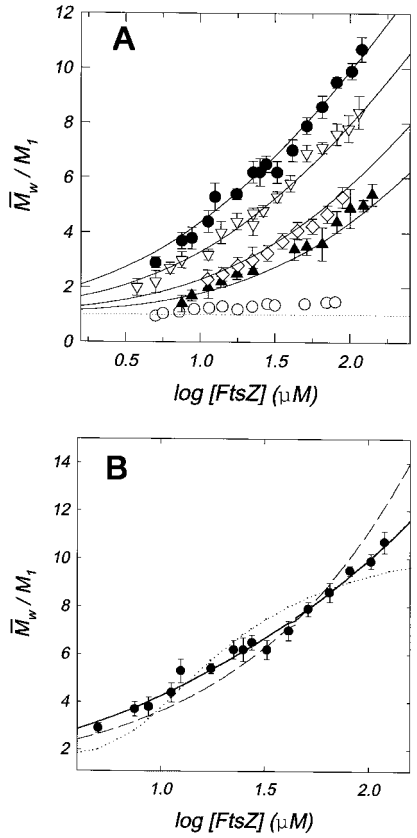

FIG. 4. **Analysis of the Mg^{2+}-induced FtsZ association.** Mg^{2+} dependence of the state of association of FtsZ ($\bar{M}_w/M_1$) upon protein concentration. *Panel A,* each symbol type represents a different Mg^{2+} concentration: *open circles* (~1 μM), *closed triangles* (1 mM), *open diamonds* (2 mM), *open inverted triangles* (5 mM), and *closed circles* (10 mM). The *solid lines* are the corresponding best fit indefinite self-association functions calculated with the inverse decay model (J = 3.32, α = 0.153, log K^*_{inf} = 4.29, n = 1); best fit curves calculated with either model are indistinguishable. *Panel B,* the symbols show the sedimentation equilibrium data obtained at 10 mM Mg^{2+}. The *solid line* corresponds to the best fit to the indefinite self-association model. The corresponding best fits to an isodesmic (*dashed line*; J = 1, log K^*_{inf} = 5.4) and to a monomer-dimer-dodecamer (*dotted line*; log K_2 = 7.9, log K_{12} = 27.7) association models, both inconsistent at a 95% level of confidence, are also plotted.

unambiguously that 1 additional mole of Mg^{2+} is bound for each protomer of FtsZ added to a growing oligomer.[5] Thus, for a given oligomer size i, the stepwise association constant K_i increases in direct proportion to the concentration of Mg^{2+} (Fig. 5, *panel A*); K_i increases an order of magnitude between 0.1 (*curve 1*) and 1 mM (*curve 2*) Mg^{2+} and another order upon raising [Mg^{2+}] to 10 mM (*curve 3*).

2. The data are inconsistent with an isodesmic model (J = 1) at a 95% level of confidence, as judged by the best fit value of χ^2 (63) (see *dotted line* in Fig. 4, *panel B*). This model assumes that the stepwise association constant K_i is independent of i. Therefore, according to our analysis, the free energy of monomer addition becomes more positive with increasing oligomer size, although by an amount that is significantly smaller than that calculated by Chatelier (70) on the basis of a simple rigid body statistical-thermodynamic model. The data are also inconsistent, within experimental precision, with defined oligomer models, such as a monomer-dimer-n-mer model (see *dotted line* in Fig. 4, *panel B*).

3. Although the values of the individual parameters K^*_{inf}, J, and α or β are not individually well determined by the data, the correlations between them required to achieve a satisfactory fit are such that the derived dependence of the stepwise association constants K_i on Mg^{2+} concentration and oligomer size is, to a very good approximation, independent of individual parameter values and even independent of the particular model employed, so long as the fit to the data is within experimental uncertainty. This is illustrated in Fig. 5, *panel A*, which shows the maximum divergence between K_i calculated from acceptable fits to the data with the two different models. For any value of i between 2 and 25, the indicated uncertainty in the absolute value of K_i amounts to less than 25% or, equivalently, an uncertainty of ~0.1 RT (60 cal/mol at room temperature) in the stepwise free energy of association.

4. The size dependence of the cumulative free energy change of i-mer assembly, ΔG_{1i} (Fig. 5, *panel B*) is well determined. This result is not entirely unexpected, as the cumulative association constants Z_i (and free energy changes) are more directly linked to the calculation of the species distribution, plotted in Fig. 5 (*panel C*), and the weight average molar mass (Equations 5 and 10).

Sedimentation Velocity Shape of FtsZ Oligomers—In order to confirm the Mg^{2+}-induced FtsZ self-association and to obtain information about the shape of the oligomers, sedimentation velocity experiments were performed. In Fig. 6, *panel A* (*curves a–d*), the $g(s^*)$ sedimentation coefficient distribution of FtsZ is plotted as a function of Mg^{2+} concentration. The sedimentation coefficient of FtsZ increases with Mg^{2+} concentration from 3.5 S (at ~1 μM Mg^{2+}) to 8.2 S (at 10 mM Mg^{2+}), with intermediate values of 5.4 and 7.4 S at 1 and 5 mM Mg^{2+}, respectively. Fig. 6, *panel B*, summarizes the available data on the dependence of the weight average sedimentation coefficient of FtsZ upon protein and Mg^{2+} concentrations.

From the combined analytical centrifugation data, and taking into account the proposed FtsZ association scheme, the shape of the Mg^{2+}-induced FtsZ was analyzed. The dependence of s_w (considering oligomer sizes up to 50-mer) with protein concentration for different structural models of FtsZ oligomers was calculated using Equations 13 and 14 in the hydrodynamic treatment described under "Theory." For a linear FtsZ oligomer with an axial spacing of 4.3 nm (23, 24, 77), this dependence is reasonably compatible with the experimental data (*solid lines*

[5] Subsequent modeling of the data was carried out with n constrained to a value of unity.

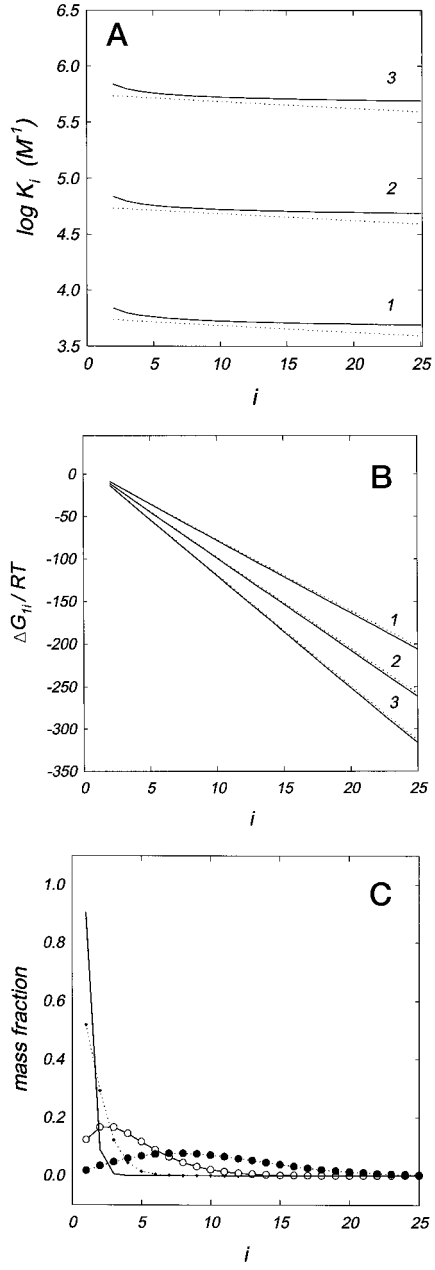

FIG. 5. **Analysis of the Mg^{2+}-induced FtsZ association.** Dependence of log K_i (*panel A*) and $\Delta G_{1i}/RT$ (*panel B*) on oligomer size and Mg^{2+} concentration, plotted for two models with distinctly different parameter sets providing close fit to experimental data. *Solid line,* inverse decay model with $J = 1.77$, $\alpha = 0.344$, log $K^{*}_{inf} = 4.59$. *Dashed line,* exponential decay model with $J = 6$, $\beta = 56.6$, log $K^{*}_{inf} = 3.96$. The Mg^{2+} concentrations plotted are 0.1 mM (*curves 1*), 1 mM (*curves 2*), and 10 mM (*curves 3*). These two parameter sets indicate the maximum spread of values obtained for a variety of best fit parameter sets in both models; all other parameter sets providing the same quality of fit yielded distributions of log K and log Z lying between the extremes indicated here (see text for details). *Panel C,* distribution of species calculated for 10 mM Mg^{2+}, at 1 (+), 10 (*open circles*), and 100 (*closed circles*) μM total FtsZ concentration. The *solid lines* are the corresponding mass fractions for 1 mM Mg^{2+} at 1 and 100 μM FtsZ (note that the value for the highest protein concentration is superimposed with the calculated distribution for 10 mM Mg^{2+} at 10 μM FtsZ).

in Fig. 6, *panels B* and *C*). The behavior for a double-stranded linear oligomer model (using for simplicity 4.3 nm as the lateral inter-protofilament spacing) deviates from the sedimentation velocity data (*dashed-dotted line* in Fig. 6, *panel C*). It is clear that a spherical FtsZ oligomer is not compatible with the experimental data (*dotted line* in Fig. 6, *panel C*). In fact, any departure from a linear oligomerization consisting of a more compact structure or a markedly flexible/curved oligomer shape would result in an increase of the s_w model values and a poorer fit to the data. Only a significant increase of the axial intermonomer spacing (up to 6 nm) could lower the average sedimentation coefficient values of the double-stranded oligomer model near the data (*short dashed line* in Fig. 6, *panel C*). However, this increasing in axial spacing is neither supported by the data available from electron microscopy (23, 24, 77) nor by the available crystal dimensions of FtsZ molecules (21). Therefore, within the accuracy of the present data and model, a single-stranded linear oligomeric structure is favored.

Qualitative Effects of Solution Variables (Ionic Strength, pH, and Ca^{2+}) on Mg^{2+}-induced FtsZ Association—The role of ionic strength on the Mg^{2+}-induced self-association of FtsZ was studied by sedimentation equilibrium. The results obtained are summarized in Table I. At 25 μM protein, the degree of association of FtsZ, equilibrated in Tris-500KCl buffer (Tris-500KCl buffer, 50 mM Tris-HCl, 500 mM KCl, pH 7.5) with 20 μM GDP and 10 mM $MgCl_2$, is not significantly larger than 2, while in the corresponding FtsZ sample at 50 mM KCl this value was around 6. Therefore, the data show that increasing the ionic strength of the solution (250–500 mM KCl) diminishes the tendency of FtsZ to self-associate, even at high Mg^{2+} concentration (5–10 mM). This effect has been confirmed by parallel sedimentation velocity experiments (Table I and Fig. 6, *panel A*). For example, the sedimentation coefficient of 25 μM FtsZ in the presence of 5 mM Mg^{2+} diminishes from 7.4 S (*profile c* in Fig. 6, *panel A*) to 4.2 S (*solid line* in Fig. 6, *panel A*) when the KCl concentration of the solution is increased from 50 to 500 mM, and it has an intermediate value (5.2 S) at 250 mM KCl (not shown).

Preliminary analytical centrifugation experiments performed in PIPES and MES buffers (pH 6.5) indicate a favored FtsZ oligomer formation. The sedimentation coefficient of FtsZ (~20 μM) in MES buffer with 1 mM Mg^{2+} is 6.8 ± 0.2 S, whereas it was only 5.4 ± 0.1 S for the equivalent sample in Tris-50KCl buffer. The presence of a minor (<10%) and faster species (~ 10 S) not observed in Tris buffer would be an indication that the scheme of FtsZ association might be different than that proposed with pH 7.5 buffer. A loss of mass observed in the sedimentation equilibrium experiments[6] suggests that these experimental conditions also affect the solubility of FtsZ, which can be compatible with the pH dependence of FtsZ polymer formation *in vitro* (Fig. 1 (44, 78)). Finally, preliminary sedimentation velocity data showed that Ca^{2+} induces FtsZ oligomer formation. For example, the sedimentation coefficient of 25 μM FtsZ increases from 3.5 ± 0.1 S (no Ca^{2+} added[4]) to 6.6 ± 0.2 S (+ 5 mM Ca^{2+}) in Tris-50KCl buffer[4] (*open circles* and *dashed line* in Fig. 6, *panel A*, respectively).

Effect of Bound Nucleotide on Mg^{2+}-induced FtsZ Association—After characterizing the Mg^{2+}-induced association of FtsZ in its GDP-bound form (the reference ground state), the effects of GTP binding were explored, because the γ-phosphate of the nucleotide switches FtsZ into the active state for assembly (Fig. 1). The nucleotide exchange method (see "Experimental Procedures") renders FtsZ with ~80–90% GTP bound when done in 0.1 mM GTP and in the absence of Mg^{2+} (~1 μM), and the protein sediments as a 3.5 ± 0.1 S species (not shown), the same as the GDP-FtsZ monomer (3.4 ± 0.1 S). However, when the divalent cation concentration was increased to 1–10 mM only GDP-FtsZ was obtained, due to GTP hydrolysis, which is compatible with the GTPase activity of FtsZ found (this work and see Refs. 15–17 and 75).

[6] J. Fernández and G. Rivas, unpublished data.

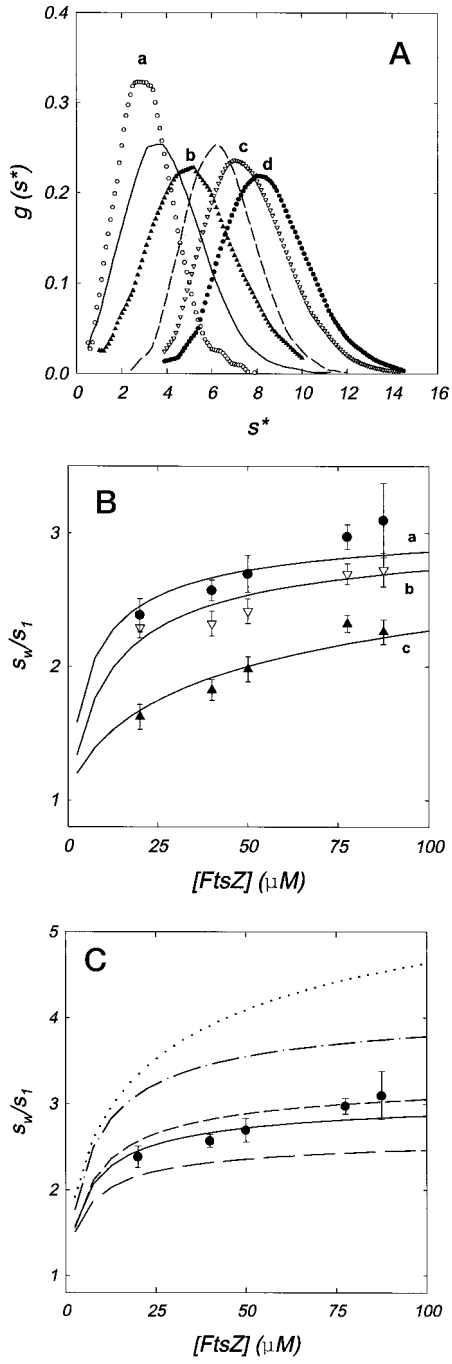

FIG. 6. **FtsZ sedimentation velocity analysis.** *Panel A,* distribution of $g(s^*)$ profiles of a fixed FtsZ concentration (20 μM) under different experimental conditions to show the following: (i) the effect of the Mg^{2+} concentration (in Tris-50KCl buffer): ~1 μM (*curve a, open circles*), 1 mM (*curve b, closed triangles*), 5 mM (*curve c, open inverted triangles*), and 10 mM Mg^{2+} (*curve d, closed circles*); (ii) the effect of ionic strength (*solid line*, in Tris-500KCl buffer with 10 mM $MgCl_2$); and (iii) the effect of Ca^{2+} (*dashed line,* Tris-50KCl buffer with 5 mM $CaCl_2$). *Panel B,* dependence of the weight average sedimentation coefficient of FtsZ upon protein concentration in Tris-50KCl buffer with 1 mM (*closed triangles*), 5 mM (*open inverted triangles*), and 10 mM Mg^{2+} (*closed circles*). The *solid lines* represent the calculated dependence of *s* with protein concentration for a linear oligomer with an axial spacing of 4.3 nm (see text for details). *Panel C,* analysis of the shape of FtsZ oligomers induced by 10 mM Mg^{2+}. The symbols show the experimental data. The different line types correspond to the calculated dependence (see text) for linear oligomers with 4.3 nm (*solid line*) and 6 nm (*long dashed line*) axial spacing, double-stranded linear oligomers with 4.3 nm (*dash-dot line*) and 6 nm (*short dashed line*) axial spacing, both with an inter-filament spacings of 4.3 nm, and an spherical oligomer (*dotted line*). Similar results were obtained at 5 mM $MgCl_2$.

To overcome these problems which precluded getting FtsZ with GTP bound in the presence of 1–10 mM Mg^{2+} at low GTP concentrations (experimental condition required to properly measure the protein with the absorption optics of the XL-A ultracentrifuge), a second approach was taken, using an FtsZ that was gently labeled with an extrinsic chromophore (FITC). The fluorescein labeling apparently did not alter the association properties of FtsZ when compared with the unlabeled protein as checked by sedimentation velocity (see legend of Fig. 7). Therefore, this FITC-FtsZ can be used to study the effect of GTP on the physical state of the protein at high GTP concentration (2 mM) by monitoring the protein in the visible region. Under these conditions a significant concentration of GTP with respect to GDP is present in the solution during the time scale of the experiment (1–2 h), as measured by HPLC and GTPase assays performed under identical conditions (not shown). The data shown in Fig. 7 indicate that GTP seems to reduce the FtsZ self-association induced by Mg^{2+}. It can be assumed that a large fraction of FtsZ is present in its GTP-bound state. If the association scheme remains the same, this would be compatible with a weakening of the monomer-monomer interaction upon GTP binding.

DISCUSSION

The role of the FtsZ protein in *E. coli* division has been described as forming part of the initial steps in the formation of the septum (4). Its assembly into the cell center forming a so-called FtsZ division ring seems to precede any other visible signs of septum formation and takes place shortly after completion of DNA replication (7). In this work we have shown that purified FtsZ associates from a monomer into Mg^{2+}-induced linear oligomers.[7] In the following discussion we propose that these interactions are the primary steps of FtsZ assembly.

The smallest association state of FtsZ in solution is a compact and globular monomer, a species whose presence is favored by moderate ionic strength and low Mg^{2+} concentrations. As in the case of tubulin, the eukaryotic homolog of FtsZ, magnesium determines the association properties of FtsZ in solution. Our data are best described by an indefinite association scheme in which the affinity of addition of a protomer gradually decreases with increasing oligomer size. In addition, protein association is linked to the binding of an additional Mg^{2+} per FtsZ association step (Fig. 4, *panel A*). The shape of the Mg^{2+}-induced FtsZ oligomers which best explains the combined analysis of the sedimentation velocity and equilibrium data is a linear single-stranded oligomeric structure. This would be compatible with the 5–10 subunits long straight protofilaments found in rotary-shadowed electron micrographs of FtsZ under nonassembly conditions (75, 77). Under assembly solution conditions single (and double-stranded) straight filaments can be visualized after negative stain electron microscopy (Fig. 1), similarly to previous observations (23, 78). Mini-rings and curved filament ends have been previously observed by electron microscopy of FtsZ polymers adsorbed onto cationic lipid, and the ring curvature has been related to either GDP or GTP being bound at the FtsZ nucleotide-binding site (23, 77, 78, 79). In our solution study we were unable to detect FtsZ mini-rings by sedimentation velocity and electron microscopy.

[7] After submission of this paper, Sossong and co-workers (92) have reported evidence suggesting that the activation of FtsZ GTPase is due to Mg^{2+}-induced oligomerization, forming dimers, trimers, and tetramers. Their sedimentation equilibrium analysis at a single speed (18,000 rpm), using a narrower range of protein concentration, in the absence and in the presence of 5 mM $MgCl_2$, is qualitatively compatible with the fact that Mg^{2+} promotes higher order linear FtsZ oligomer formation (this study). A similar Mg^{2+}-induced CD change (Fig. 2*B*) has been observed.

TABLE I
Mg^{2+}-induced FtsZ self-association at 50 and 500 mM KCl
Experiments were performed at 8,000 (sedimentation equilibrium) and 50,000 rpm (sedimentation velocity) and 20 °C, with ~20 μM FtsZ.

$[Mg^{2+}]^a$	$\overline{M}_w$ 50 mM KCl	$\overline{M}_w$ 500 mM KCl	$s_{20,w}$ (S) 50 mM KCl	$s_{20,w}$ (S) 500 mM KCl
~1 μM	51,400 ± 4,000[b]	46,000 ± 3,000	3.5 ± 0.1	3.4 ± 0.1
1 mM	88,700 ± 12,100	55,000 ± 4,000	5.4 ± 0.2	3.8 ± 0.1
5 mM	166,000 ± 16,500	74,000 ± 6,000	7.5 ± 0.3	4.2 ± 0.2[c]
10 mM	226,000 ± 18,000	86,000 ± 9,000	8.2 ± 0.3	ND[d]

[a] Buffer, 50 mM Tris-HCl, 20 μM GDP, pH 7.5, with 500 mM KCl.
[b] Monomer M_r is 40,300.
[c] At 250 mM KCl the corresponding sedimentation coefficient is 5.4 ± 0.2 S.
[d] ND, not determined.

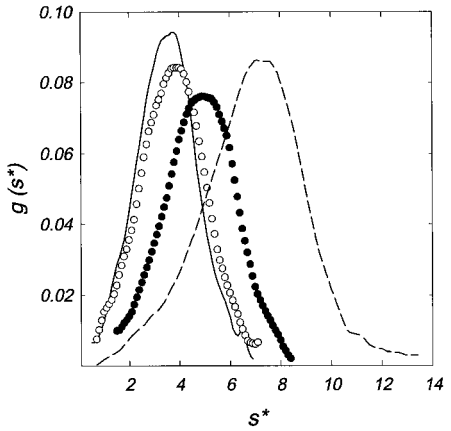

FIG. 7. **Effect of nucleotides on the Mg^{2+}-induced FtsZ self-association.** Sedimentation velocity profiles of FITC-FtsZ (~18 μM, in Tris-50KCl buffer) taken at 50,000 rpm and 20 °C, in the presence of 20 μM GDP (*solid line,* ~1 μM Mg^{2+} ($s_{20,w}$ = 3.7 ± 0.2 S); *dashed line,* 5 mM Mg^{2+} ($s_{20,w}$ = 7.0 ± 0.2 S)) or 2 mM GTP (*open circles,* ~1 μM Mg^{2+} ($s_{20,w}$ = 3.8 ± 0.3 S); *closed circles,* 5 mM Mg^{2+} ($s_{20,w}$ = 5.9 ± 0.3 S)). At 1 mM Mg^{2+}, the corresponding sedimentation coefficients in 20 μM GDP and 2 mM GTP were 5.3 ± 0.2 and 4.6 ± 0.2 S, respectively.

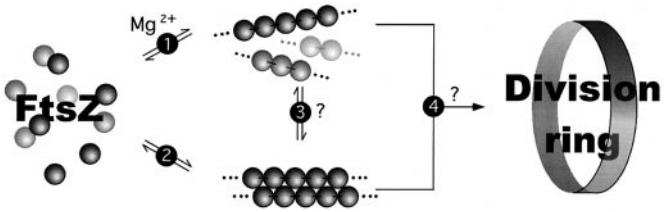

SCHEME 1. **A model scheme that summarizes the results and implications of this work.** The reaction studied is the indefinite Mg^{2+}-induced association of FtsZ into linear oligomers (*reaction 1*). It is proposed that this is a predominant interaction in the cooperative nucleated condensation polymerization of FtsZ (simply represented as the formation of a double-stranded filament in *reaction 2*, which is based on previous results (Refs. 23, 75, 77, 78), and this work, and hypothetical *reaction 3*), and that cellular modulation of these interactions (*pathway 4*) would result in the correct formation of the *Z*-ring during bacterial division (see text).

This could be explained if the FtsZ oligomers were less flexible than in the case of tubulin, impeding the curvature required for the end-closure reaction in solution.

The endwise association of αβ-tubulin dimers induced by Mg^{2+} proceeds by an indefinite association mechanism (34, 35). Linear oligomers equivalent to fragments of microtubule protofilaments are formed. Therefore, the energetics of the linear oligomerization of FtsZ in solution provides a strong counterpart to the tubulin-like structural model of FtsZ protofilaments (23, 24, 78, 80). FtsZ oligomer formation is promoted by reducing the ionic strength. This is also the case in tubulin, where microtubule assembly is favored at low salt conditions and is inhibited by salt (KCl or NaCl) at concentrations in excess of 100–150 mM (39, 81). Similarly to tubulin (41), the self-association of FtsZ is apparently stronger with GDP than with GTP bound at the nucleotide site. In the case of FtsZ this nucleotide effect seems to be a weakening of the monomer-monomer association, whereas for tubulin it was suggested to be due to the conformation of the GDP-liganded protein being more favorable for the closure reaction (41). The effect is intriguing, since in both cases the GTP-liganded protein is the active species forming larger polymers. FtsZ oligomers and polymers, observed in this work under different solution conditions of temperature and buffer composition, might be alternative association pathways as in the case of tubulin (33, 41) (see Scheme 1).

We have found that oligomerization depends to a large extent on FtsZ concentration and Mg^{2+} ions, and it is favored by low ionic strength. The estimates for the number of FtsZ copies present in the cell (from 5,000 to 20,000 (6, 75, 82)) would indicate that FtsZ is at a concentration of ~10 μM; the physiological free concentration of Mg^{2+} is ~1–2 mM (83); the intracellular pH is around 7.6–7.8 (84), and the total intracellular K^+ concentration ranges about 0.1 to 1 M (85). By taking into account these physiological concentrations of protein and ions inside the cell, our results summarized in Fig. 4, *panel A*, would suggest that under physiological micro-solute conditions isolated FtsZ is reluctant to associate. This would be consistent with earlier data that indicated that the majority of the FtsZ molecules are found in the soluble fraction of the cell (82), and with a previous report by Jones and Holland (86) that an extended sonic treatment of the samples at 10 mM Mg^{2+} was needed for the association of FtsZ to the membrane fraction of maxicells.

However, there are other important factors that might regulate the state of association and assembly of FtsZ *in vivo*. (i) Excluded volume effects due to crowding (87, 88) at the high macromolecular concentrations estimated for *E. coli* cytoplasm (several hundreds of mg/ml; Refs. 85 and 89) would favor that FtsZ exists in an aggregated/oligomeric state inside the cell. Zimmerman and Trach (89) have discussed the effects of such a high volume occupancy inside the cell upon the association equilibria of a protein of the size of FtsZ monomer (40,000) and calculated that if the protein is in a mixture of monomers and dimers (or tetramers) at equilibrium the association constant would be shifted 10–40-fold (or 10^3 to 10^5) toward dimerization (or tetramer formation). (ii) A large volume of the cell interior is occupied by the nucleoid, what has led to conjecture, following the nucleoid occlusion model of Woldringh (90), that septation cannot occur in regions occupied by the nucleoid. Migration of FtsZ (due to electrostatic repulsions) toward nucleoid-free regions of the cell (namely the poles and after segregation has taken place, the cell center) would result in a substantial increase in local concentration of FtsZ which also could facilitate FtsZ oligomer formation. Activation of the MinCD division inhibitor would prevent division at the poles, whereas such a mechanism would not be operating at mid-cell. However, recent data indicating that the FtsZ division ring is visible prior to the estimated time of nucleoid segregation would make this

assumption unlikely (7). (iii) The FtsZ oligomers involved in the formation of the ring might be clustered by specific binding to another protein or structure, presently unknown, that can be further stabilized by FtsA and Zip A, given their proven interaction with FtsZ (13, 91).

A simple way to summarize the implications of the results presented in this work is shown in Scheme 1. It is proposed that the primary interaction for FtsZ assembly *in vivo* is the relatively weak endwise association of FtsZ monomers, which is induced by Mg^{2+}, and leads as well to oligomer formation. Binding of GTP and changes in solution conditions (temperature, lowering pH) promote additional FtsZ-FtsZ interactions that would result in a cooperative bidimensional polymer assembly. Modulation of the energetics of self-association by additional factors, such as molecular crowding, nucleoid occlusion, or specific molecular interactions with other cellular components active in septation have to be invoked to explain FtsZ assembly into a division ring.

Acknowledgments—We especially thank Dr. Fernando Díaz for discussions and suggesting and performing the stopped-flow measurements; and Javier Fernández for help in FtsZ purification, sedimentation equilibrium, and for the preparation of Fig. 1. We also thank Dr. Consuelo López-Zúmel for the use of the stopped-flow instrument; Dr. Francisco Gavilanes, for performing the amino acid analysis; Dr. Pilar Lillo, for helpful comments on FtsZ quantitation; and Dr. Carlos Alfonso for assistance in the analytical centrifugation experiments.

REFERENCES

1. Stephens, R. S., Kalman, S., Lammel, C., Fan, J., Marathe, R., Aravind, L., Mitchell, W., Olinger, L., Tatusov, R. L., Zhao, Q., Koonin, E. V., and Davis, R. W. (1998) *Science* **282,** 754–759
2. Kalman, S., Mitchell, W., Marathe, R., Lammel, C., Fan, J., Hyman, R. W., Olinger, L., Grimwood, J., Davis, R. W., and Stephens, R. S. (1999) *Nat. Genet.* **21,** 385–389
3. Bramhill, D. (1997) *Annu. Rev. Cell Dev. Biol.* **13,** 395–424
4. Lutkenhaus, J., and Addinall, S. G. (1997) *Annu. Rev. Biochem.* **66,** 93–116
5. Vicente, M., and Errington, J. (1996) *Mol. Microbiol.* **20,** 1–7
6. Bi, E., and Lutkenhaus, J. (1991) *Nature* **354,** 161–164
7. den Blaauwen, T., Buddelmeijer, N., Aarsman, M. E., Hameete, C. M., and Nanninga, N. (1999) *J. Bacteriol.* **181,** 5167–5175
8. Margolin, W. (1998) *Trends Microbiol.* **6,** 233–238
9. Rothfield, L. I., and Justice, S. S. (1997) *Cell* **88,** 581–584
10. Mukherjee, A., Cao, C., and Lutkenhaus, J. (1998) *Proc. Natl. Acad. Sci. U. S. A.* **95,** 2885–2890
11. Rothfield, L. I., and Zhao, C. R. (1996) *Cell* **84,** 183–186
12. Levin, P. A., Kurtser, I. G., and Grossman, A. D. (1999) *Proc. Natl. Acad. Sci. U. S. A.* **96,** 9642–9647
13. Hale, C. A., and de Boer, P. A. J. (1997) *Cell* **88,** 175–185
14. RayChaudhuri, D. (1999) *EMBO J.* **18,** 2372–2383
15. de Boer, P., Cossley, R., and Rothfield, L. (1992) *Nature* **359,** 254–256
16. Mukherjee, A., Dai, K., and Lutkenhaus, J. (1993) *Proc. Natl. Acad. Sci. U. S. A.* **90,** 1053–1057
17. RayChaudhuri, D., and Park, J. T. (1992) *Nature* **359,** 251–254
18. Wang, X., and Lutkenhaus, J. (1993) *Mol. Microbiol.* **21,** 313–319
19. de Pereda, J. M., Leynadier, D., Evangelio, J. A., Chacon, P., and Andreu, J. M. (1996) *Biochemistry* **35,** 14203–14215
20. Erickson, H. P. (1995) *Cell* **80,** 367–370
21. Löwe, J., and Amos, L. A. (1998) *Nature* **391,** 203–206
22. Nogales, E., Wolf, S. G., and Downing, K. (1998) *Nature* **391,** 199–203
23. Erickson, H. P., Taylor, D., Taylor, K., and Bramhill, D. (1996) *Proc. Natl. Acad. Sci. U. S. A.* **93,** 519–523
24. Löwe, J., and Amos, L. A. (1999) *EMBO J.* **18,** 2364–2371
25. Mukherjee, A., and Lutkenhaus, J. (1994) *J. Bacteriol.* **176,** 2754–2758
26. Mukherjee, A., and Lutkenhaus, J. (1998) *EMBO J.* **17,** 462–469
27. Mukherjee, A., and Lutkenhaus, J. (1999) *J. Bacteriol.* **181,** 823–832
28. Yu, X., and Margolin, W. (1997) *EMBO J.* **16,** 5455–5463
29. Desai, A., and Mitchison, T. J. (1997) *Annu. Rev. Cell Dev. Biol.* **13,** 83–117
30. Menéndez, M., Rivas, G., Díaz, J. F., and Andreu, J. M. (1998) *J. Biol. Chem.* **273,** 167–176
31. Correia, J. J., Baty, L. T., and Williams, R. C., Jr. (1987) *J. Biol. Chem.* **262,** 17278–17284
32. Correia, J. J., Beth, A., and Williams, R. C., Jr. (1988) *J. Biol. Chem.* **263,** 10681–10686
33. Díaz, J. F., Andreu, J. M., Diakun, G., Towns-Andrews, E., and Bordas, J. (1996) *Biophys. J.* **70,** 2408–2420
34. Frigon, R. P., and Timasheff, S. N. (1975) *Biochemistry* **14,** 4559–4566
35. Frigon, R. P., and Timasheff, S. N. (1975) *Biochemistry* **14,** 4567–4573
36. Shearwin, K. E., and Timasheff, S. N. (1992) *Biochemistry* **33,** 885–893
37. Carlier, M. F. (1991) *Curr. Opin. Cell Biol.* **3,** 12–17
38. Dreschel, D. N., and Kirschner, M. W. (1994) *Curr. Biol.* **4,** 1053–1061
39. Lee, J. C., and Timasheff, S. N. (1977) *Biochemistry* **16,** 1754–1764
40. Díaz, J. F., Pantos, E., Bordas, J., and Andreu, J. (1994) *J. Mol. Biol.* **238,** 214–225
41. Howard, W. D., and Timasheff, S. N. (1986) *Biochemistry* **25,** 8292–8300
42. Melki, R., Carlier, M. F., Pantaloni, D., and Timasheff, S. N. (1989) *Biochemistry* **28,** 9143–9152
43. Müller-Reichert, T., Chrétien, D., Severin, F., and Hyman, A. A. (1998) *Proc. Natl. Acad. Sci. U. S. A.* **95,** 3661–3666
44. Mukherjee, A., and Lutkenhaus, J. (1998) *Methods Enzymol.* **298,** 296–305
45. Williams, R. C., and Lee, J. C. (1982) *Methods Enzymol.* **85,** 376–385
46. Sambrook, J., Fritsch, E. F., and Maniatis, T. (1989) *Molecular Cloning: A Laboratory Manual,* 2nd Ed., Cold Spring Harbor Laboratory, Cold Spring Harbor, NY
47. Blattner, F. R., Plunkett, G., III, Bloch, C. A., Perna, N. T., Burland, V., Riley, M., Collado-Vides, J., Glasner, J. D., Rode, C. K., Mayhew, G. F., Gregor, J., Davis, N. W., Kirkpatrick, H. A., Goeden, M. A., Rose, D. J., and Shao, Y. (1997) *Science* **277,** 1453–1462
48. Díaz, J. F., and Andreu, J. M. (1993) *Biochemistry* **32,** 2747–2755
49. Fasman, G. D., ed. (1992) *Practical Handbook of Biochemistry and Molecular Biology*, pp. 81–82, CRC Press Inc., Boca Raton, FL
50. Pace, C. N., and Schmid, F. X. (1997) in *Protein Structure: A Practical Approach* (Creighton, T., ed) 2nd Ed., pp. 253–259, Oxford University Press, Oxford
51. Ozols, J. (1990) *Methods Enzymol.* **182,** 587–601
52. Martin, M. T., and Shapiro, R. (1988) *Methods Enzymol.* **158,** 365–370
53. Boss, C. B., and Fredeen, K. J. (1997) *Concepts, Instrumentation, and Techniques in Inductively Coupled Plasma Optical Emission Spectrometry*, Perkin-Elmer Corp., Norwalk, CT
54. Hoenig, M., Lee, R. J., and Ferguson, D. C. (1989) *J. Biochem. Biophys. Methods* **19,** 249–252
55. Lanzetta, P. A., Alvarez, L. J., Reinach, P. S., and Candia, O. A. (1979) *Anal. Biochem.* **100,** 95–97
56. Peterman, B. F. (1979) *Anal. Biochem.* **93,** 442–444
57. Minton, A. P. (1994) in *Modern Analytical Ultracentrifugation* (Schuster, T., and Laue, T., eds) pp. 81–93, Birkhauser Boston, Inc., Cambridge, MA
58. Laue, T. M., Shah, B. D., Ridgeway, T. M., and Pelletier, S. L. (1992) in *Analytical Ultracentrifugation in Biochemistry and Polymer Science* (Harding, S., Rowe, A., and Horton, J., eds) pp. 90–125, Royal Society of Chemistry, Cambridge, UK
59. Muramatsu, N., and Minton, A. P. (1989) *J. Mol. Recognit.* **1,** 166–171
60. Philo, J. S. (1997) *Biophys. J.* **72,** 435–444
61. Stafford, W. F. (1994) *Methods Enzymol.* **240,** 478–501
62. Lobert, S., Frankfurter, A., and Correia, J. J. (1995) *Biochemistry* **34,** 8050–8060
63. Press, W. H., Flannery, B. P., Teukolsky, S. A., and Vetterling, W. T. (1989) *Numerical Recipes in Pascal: The Art of Scientific Computing*, Cambridge University Press, Cambridge, MA
64. Yang, J. T., Chuen-Shang, C. W., and Martinez, H. M. (1986) *Methods Enzymol.* **130,** 208–269
65. Perczel, A., Parck, K., and Fasman, G. D. (1992) *Anal. Biochem.* **203,** 83–93
66. Waggoner, A. (1995) *Methods Enzymol.* **246,** 362–373
67. Wyman, J. (1964) *Adv. Protein Chem.* **19,** 223–286
68. Tanford, C. (1970) *Adv. Protein Chem.* **24,** 1–95
69. Record, M. T., Jr., Anderson, C. F., and Lohman, T. M. (1978) *Q. Rev. Biophys.* **11,** 103–178
70. Chatelier, R. C. (1987) *Biophys. Chem.* **28,** 121–128
71. Bloomfield, V., Dalton, W. O., and van Holde, K. E. (1967) *Biopolymers* **5,** 135–148
72. Cantor, C. R., and Schimmel, P. R. (1980) *Biophysical Chemistry,* Vol. 2, pp. 539–590, W. H. Freeman & Co., San Francisco, CA
73. Cooper, J. A., and Pollard, T. D. (1982) *Methods Enzymol.* **85,** 182–210
74. Korn, E. D. (1982) *Physiol. Rev.* **62,** 672–737
75. Lu, C., Stricker, J., and Erickson, H. P. (1998) *Cell Motil. Cytoskeleton* **40,** 71–86
76. Andreu, J. M., and Timasheff, S. N. (1986) *Methods Enzymol.* **130,** 47–59
77. Lu, C., and Erickson, H. P. (1998) *Methods Enzymol.* **298,** 305–313
78. Erickson, H. P., and Stoffler, D. (1996) *J. Cell Biol.* **135,** 5–8
79. Erickson, H. P. (1997) *Trends Cell Biol.* **7,** 362–367
80. Nogales, E., Whittaker, M., Milligan, R. A., and Downing, K. H. (1999) *Cell* **96,** 79–88
81. Olmsted, J. B., and Borisy, G. G. (1973) *Biochemistry* **12,** 4282–4289
82. Pla, J., Sánchez, M., Palacios, P., Vicente, M., and Aldea, M. (1991) *Mol. Microbiol.* **5,** 1681–1686
83. Chang, C. F., Shuman, H., and Somlyo, A. P. (1986) *J. Bacteriol.* **167,** 935–939
84. Padan, E., and Schudilner, S. (1987) *J. Membr. Biol.* **95,** 189–198
85. Record, M. J., Jr., Courtenay, E. S., Cayley, S., and Guttman, H. J. (1998) *Trends Biochem. Sci.* **23,** 190–194
86. Jones, C. A., and Holland, I. B. (1984) *EMBO J.* **3,** 1181–1183
87. Zimmerman, S. B., and Minton, A. P. (1993) *Annu. Rev. Biophys. Biomol. Struct.* **22,** 27–65
88. Minton, A. P. (1997) *Curr. Opin. Biotechnol.* **8,** 65–69
89. Zimmerman, S. B., and Trach, S. O. (1991) *J. Mol. Biol.* **222,** 599–620
90. Woldringh, C. L., Mulder, E., Huls, P. G., and Vischer, N. (1991) *Res. Microbiol.* **142,** 309–320
91. Wang, X., Huang, J. A., Mukherjee, A., Cao, C., and Lutkenhaus, J. (1997) *J. Bacteriol.* **179,** 5551–5559
92. Sossong, T. M., Jr., Brigham-Burke, M. R., Hensley, P., and Pearce, K. H., Jr. (1999) *Biochemistry* **38,** 14843–14850